M&C 2017 - International Conference on Mathematics & Computational Methods Applied to Nuclear Science & Engineering, Jeju, Korea, April 16-20, 2017, on USB (2017)

Coupled Burnup Calculations with the Serpent 2 Monte Carlo Code

Ville Valtavirta, Jaakko Leppänen

VTT Technical Research Centre of Finland, Kivimiehetie 3, FI-02150 Espoo, Finland
ville.valtavirta@vtt.fi, jaakko.leppanen@vtt.fi

Abstract - *This article describes the implementation of a burnup scheme with coupled fuel behavior feedback into the Monte Carlo code Serpent 2. The new capabilities are applied to estimate the effects of typical simplifications concerning the fuel temperature distribution in the burnup history part of group constant generation. A set of group constants are generated for an assembly of the EPR by executing the burnup history calculation with either an assembly wide constant effective fuel temperature or realistic pin-wise fuel temperature distributions provided by a coupling to an external fuel performance solver. The differences in nuclide concentrations and generated group constants are quantified and the benefits of using a separate effective temperature for burnable absorber rods is investigated.*

I. INTRODUCTION

Two major focus areas of the development of the Serpent 2 Monte Carlo code [1] have been spatial homogenization for group constant generation applications and coupled multi-physics calculations. This paper is situated at the interface between the two applications as the multi-physics capabilities of Serpent 2 are used to estimate the errors resulting from some of the common simplifications applied to the fuel temperature distribution in the burnup part of group constant generation.

This article will describe the coupled burnup approach in Serpent 2, which is based on the Stochastic Implicit Euler burnup scheme with thermal feedback [2]. The coupled burnup capabilities will be used to study the effect that a realistic fuel temperature distribution will have on the nuclide compositions calculated in the burnup part of group constant generation and how the effects on the nuclide compositions are reflected to the generated group constants. The comparison will be done in the context of group constants required to simulate the initial cycle of the EPR as described in [3] with the ARES core simulator [4].

This paper will focus on the differences seen in the nuclide compositions and generated group constants on assembly level, while a separate journal article has been submitted [5], where the effects on the solution obtained with the ARES core simulator are also addressed.

II. THEORY

1. The Serpent Monte Carlo code

The Serpent[1] Monte Carlo code [1] is a relatively young continuous energy Monte Carlo reactor physics burnup code with recent applications in radiation shielding, multi-physics and fusion neutronics. The code is currently used in more than 160 universities and research organizations for reactor physics applications ranging from homogenized group constant generation to burnup calculations and the modeling of small research reactor cores to multi-physics calculations with couplings to various thermal–hydraulics, CFD and solid-mechanics tools. Serpent has been developed at VTT Technical Research Centre of Finland since 2004 and the current development version, Serpent 2, has notably diversified the applications of the code. The two main areas of development for the new code version have been spatial homogenization and multi-physics applications, both of which are shortly described as this study lies in the boundary between the two.

A. Spatial Homogenization with Serpent 2

Serpent has the capability to produce homogenized group constants used by core simulator and transient analysis codes based on nodal diffusion methods. This includes homogenized reaction cross sections, scattering matrices, diffusion coefficients, discontinuity factors, time constants and production and absorption cross sections for fission product poisons ^{135}Xe and ^{149}Sm and their precursors. The calculation routines are based on standard Monte Carlo cell flux and surface current tallies, and two deterministic solvers used to obtain B_1 leakage-corrected cross sections and discontinuity factors for geometries homogenized without reflective boundary conditions. Full description of the methodology is found in [6], and not repeated here.

B. Multi-Physics Capabilities of Serpent 2

Serpent 2 has been designed for multi-physics applications. During the development of the code in the 2010's, several multi-physics specific features have been designed and added to the code. While these features are not discussed in detail here, it should be summarized that Serpent 2 is capable of modeling materials with arbitrarily refined or even continuous temperature [7, 8] and density [9] distributions in steady-state [10], burnup [11] and time dependent [12] simulations. Furthermore, Serpent is able to exchange data with external solvers during the coupled calculation Picard-iteration using various multi-physics interface file formats [13, 10].

The interface format used in this study to exchange data between Serpent and the fuel performance code ENIGMA is specifically designed for data exchange between Serpent and fuel performance codes using the so-called 1.5 dimensional geometry representation, i.e. axisymmetric (r,z) coordinate system with the fuel rods consisting of loosely coupled axial

[1] For a complete description of the code and the latest news, see the project Web site: http://montecarlo.vtt.fi

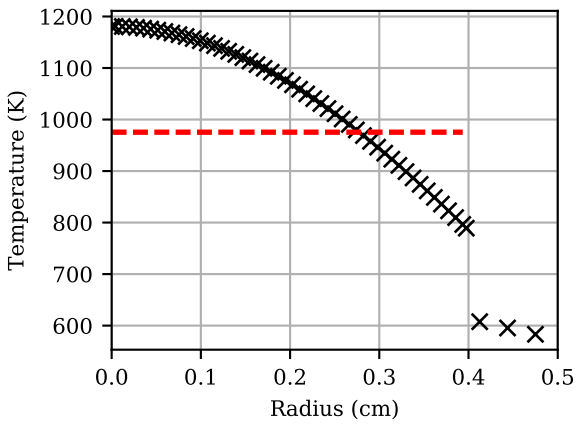

Fig. 1. Simplifaction by collapsing the radial fuel temperature distribution (black x) to a single pin-wise effective fuel temperature (red dashed line, here radial volume averaged fuel temperature).

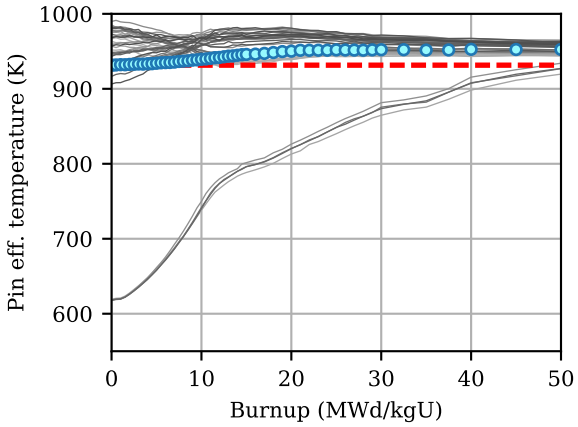

Fig. 2. Simplifaction by collapsing the pin-wise effective temperatures (gray lines) to an assembly wise effective temperature (cyan o, here assembly volume averaged fuel temperature). A further simplifaction is typically made by assuming this assembly wise effective temperature is constant throughout the burnup calculation (red dashed line, here assembly volume averaged fuel temperature at zero burnup). This assembly contains burnable absorber (BA) pins that have a low effective fuel temperature at low burnups.

zones with a separate radial fuel behavior solution in each axial zone. Using this interface format Serpent will read in radial temperature and strain distributions at the various axial zones of different fuel rods and output the fission power distribution tallied with a user specified axial and radial binning [10, 11].

2. Burnup Calculation as a Part of Group Constant Generation

Group constant generation for nodal codes typically includes running an assembly burnup calculation (history calculation) with specified history variables such as moderator temperature and boron concentration to obtain a representative nuclide composition for each point in the burnup history that the group constants are generated for. These nuclide concentrations are then used in separate assembly level calculations (branch calculations), where homogenized group constants are calculated for the assembly at specific burnups and momentary variations such as momentary fuel or coolant temperature.

Three simplifications are typically made regarding the fuel temperature distribution in the burnup calculation:

1. The radial temperature distribution in a fuel rod spanning some hundreds of Kelvins between pellet surface and centerline is collapsed into a single, effective, radially constant temperature (Fig. 1).

2. All of the different fuel rods in an assembly are set to use the same effective temperature, thus suppressing the variation of temperatures between different lattice positions and fuel types (From gray lines to cyan (o) in Fig. 2). This is a significant simplification when some of the rods in the assembly contain burnable absorber (BA).

3. The effective temperature is set to stay constant throughout the fuel life, regardless of the changes in the fuel temperatures as a function of burnup (From cyan (o) to red dashed line in Fig. 2).

Transforming the radial fuel temperature distribution into a radially constant effective temperature will lead to the overestimation of the temperature at the pellet surface and the underestimation of the temperature at the pellet inner parts. This leads to the overestimation of the width of the resonances in the nuclear cross sections for the regions close to the pellet surface, which leads to an increase in ^{238}U radiative capture and thus in ^{239}Pu production (See, for example, [10]). In the inner parts of the pellet the effect is reversed.

The choice of a single effective temperature for the whole assembly overestimates the temperatures at burnable absorber rods, especially during the beginning of the fuel life. This will, again, lead to the increased breeding of fissile ^{239}Pu in the burnable absorber rods. Keeping the assembly fuel temperature constant throughout the fuel life is less of an approximation if the power level is assumed to be constant, which is a major approximation in itself. While the radial fuel temperature distribution changes during the fuel life due to the decrease in the fuel thermal conductivity associated with increasing burnup and the slow closing of the gas gap between the pellet and the cladding, there are only small changes in most of the rod effective temperatures (see Fig.2) during the irradiation. The burnable absorber rods are naturally an exception, their effective fuel temperature changing with hundreds of Kelvins during irradiation.

In this work, the effects of these simplifications are estimated by modeling the accurate fuel temperatures explicitly with Serpent. This can be achieved by using the TMS temperature treatment [7] technique to handle the complex fuel temperature distributions, whereas the fuel behavior multiphysics interface of Serpent is used to bring in the realistic fuel temperature profile for each rod from a fuel performance code. One additional implementation was required, however,

namely a burnup scheme that can handle feedback not only from neutronics, but also from the changing fuel temperatures.

III. IMPLEMENTATION OF A COUPLED BURNUP SCHEME WITH FUEL BEHAVIOR FEEDBACK

Several advanced burnup schemes exist that consider the thermal feedback as a part of the coupled iteration scheme between neutronics and fuel depletion. These include the Stochastic Implicit Euler (SIE) scheme with thermal feedback [2], the Stochastic Implicit Midpoint (SIMP) scheme with thermal feedback [14] and the Stochastic Semi-Implicit Substep methodology with thermal feedack [15]. Due to the Stochastic Implicit Euler scheme without thermal feedback being previously implemented in Serpent [16], it was chosen as the coupled burnup scheme for this work. The implementation was extended to account for thermal feedback as described in [2]. The original description in [2] included the (thermal-hydraulic) solution for the coolant nuclide field $\mathbf{N}_\mathrm{C}$ as the solution coupled to the neutron transport solution. In this study the coolant conditions are held constant and the thermal feedback from the coolant was replaced with the solution for the fuel behavior $\mathbf{T}_\mathrm{F}$, which includes the temperature and thermal expansion distributions in each fuel rod.

The coupled burnup scheme is described in Table I. The burnup scheme starts from the initial nuclide density and fuel behavior solution for the steady state at zero burnup (step 1). The initial estimate for the transmutation cross sections and the neutron flux is obtained with a transport solution of the zero-burnup system (step 2). The first estimate for the nuclide concentrations at each burnup point is obtained using the explicit Euler method (step 4). The further iterations will always use the implicit Euler method (step 9). The first estimate for the fuel behavior solution at each burnup point is also obtained using the power distribution from the previous burnup point (step 5). After the initial estimate for the coupled solution at the burnup point has been obtained, it can be updated using several iterations of the SIE iteration loop (steps 7–10). On each iteration a new transport solution for the end-of-step system is obtained (step 7), after which the neutron flux, the power distribution and the transmutation cross sections are relaxed using the stochastic approximation based solution relaxation (step 8), which in this work amounted to simple averaging of each distribution over the iterations. After the new relaxed distributions have been obtained for the current burnup point, the depletion solution and the fuel behavior solution are updated (steps 9 and 10). For step 10, the relaxed power distribution is passed to the fuel behavior solver.

When a specified number of iterations has been simulated, the nuclide concentrations, the fuel behavior solution and the neutron transport solution will be considered to be the representative solution for the current burnup point (steps 12-14) and the algorithm will move to the next burnup point by using the explicit Euler method to provide a prediction for the next depletion solution (step 4).

1: **input:** $\mathbf{N}_{\mathrm{F},0}$, $\mathbf{T}_{\mathrm{F},0}$
2: $\phi_0 \leftarrow \phi_B(\mathbf{N}_{\mathrm{F},0}, \mathbf{T}_{\mathrm{F},0})$
3: **for** $i \leftarrow 0, 1, \ldots$ **do**
4: $\quad \mathbf{N}^{(0)}_{\mathrm{F},i+1} \leftarrow \mathbf{N}_{\mathrm{F},i} \exp\left[\mathbb{M}(\phi_i)\Delta t\right]$
5: $\quad \mathbf{T}^{(0)}_{\mathrm{F},i+1} \leftarrow \mathbf{F}(\phi_i)$
6: $\quad$ **for** $n \leftarrow 1, 2, \ldots, c$ **do**
7: $\quad\quad \phi^{(n)}_{i+1} \leftarrow \phi_B(\mathbf{N}^{(n-1)}_{\mathrm{F},i+1}, \mathbf{T}^{(n-1)}_{\mathrm{F},i+1})$
8: $\quad\quad \overline{\phi}^{(n)}_{i+1} \leftarrow \sum_{j=1}^{n} \phi^{(j)}_{i+1}/n$
9: $\quad\quad \mathbf{N}^{(n)}_{\mathrm{F},i+1} \leftarrow \mathbf{N}_{\mathrm{F},i} \exp[\mathbb{M}(\overline{\phi}^{(n)}_{i+1})\Delta t]$
10: $\quad\quad \mathbf{T}^{(n)}_{\mathrm{F},i+1} \leftarrow \mathbf{F}(\overline{\phi}^{(n)}_{i+1})$
11: $\quad$ **end for**
12: $\quad \mathbf{N}_{\mathrm{F},i+1} \leftarrow \mathbf{N}^{(c)}_{\mathrm{F},i+1}$
13: $\quad \mathbf{T}_{\mathrm{F},i+1} \leftarrow \mathbf{T}^{(c)}_{\mathrm{F},i+1}$
14: $\quad \phi_{i+1} \leftarrow \overline{\phi}^{(c)}_{i+1}$
15: **end for**

TABLE I. The Stochastic Implicit Euler method with relaxation of the neutron flux and fuel behavior feedback. The thermal hydraulic solution for the coolant $\mathbf{N}_\mathrm{C}$ in [2] has been replaced with the fuel behavior solution $\mathbf{T}_\mathrm{F}$.

Non-BA rods:	
Uranium enrichment	3.0 wt %
Fuel density	10.307 g cm^{-3}
BA rods:	
Uranium enrichment	0.25 wt %
Gd_2O_3 content	8.0 wt %
Fuel density	10.307 g cm^{-3}
Geometry:	
Pellet radius	0.3975 cm
Cladding inner radius	0.4125 cm
Cladding outer radius	0.4750 cm
Rod pitch	1.26 cm

TABLE II. Basic information concerning the fuel materials and assembly geometry.

IV. ESTIMATING THE EFFECTS FROM FUEL TEMPERATURE SIMPLIFICATIONS IN GROUP CONSTANT GENERATION

The generation of all required group constants for ARES for the first cycle of the EPR requires covering four different assembly types, nine history variations and 21 or 1 branch variations at 15 burnup points. In this article the analysis will be focused on a single assembly type using a single history variation and the group constants will be calculated only for the nominal branch.

The assembly type chosen for the comparison is shown in Figure 3 and the basic information regarding the fuel materials and fuel rod geometry are given in Table II. The history case chosen for the comparison used a moderator temperature of 583 K and a moderator boron concentration of 650 ppm. The nominal branch used for the group constant generation used a momentary fuel temperature of 900 K a momentary temperature of 583 K and a momentary moderator boron concentration of 0 ppm.

In order to quantify the effects of the effective temperature

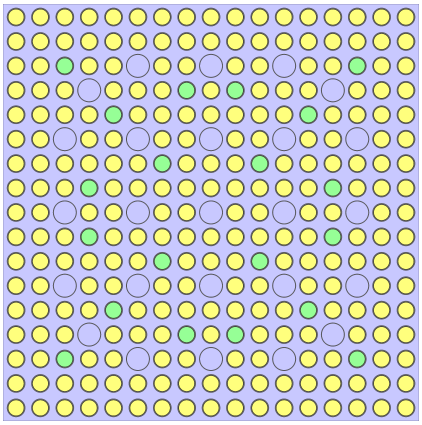

Fig. 3. The assembly type chosen for the comparison contains 20 burnable absorber pins with gadolinia mixed into the fuel.

simplification on the produced group constants, the group constant generation was executed in two ways that differed only in the fuel temperature distribution used in the burnup calculation. The first way (reference model) used the coupled methodology to execute the group constant generation for each history case in three parts:

1. Solve an initial guess for the temperature distribution in the assembly at zero burnup by running a coupled Serpent–ENIGMA simulation in steady state. The initial fuel behavior solution was calculated using 10 coupled calculation iterations.

2. Run the coupled burnup calculation using the *detailed radial temperature fields* provided by ENIGMA for each fuel rod based on the detailed power distribution tallied by Serpent. Each burnup step used 16 iterations of the SIE algorithm.

3. Using the nuclide compositions from the burnup calculation, generate the group constants using a *flat assembly-wide fuel temperature* of 900 K.

The uncoupled calculation sequence (effective model) was very similar:

1. Run the coupled burnup calculation using a *flat assembly-wide fuel temperature profile* of 900 K. Each burnup step used 16 iterations of the SIE algorithm.

2. Using the nuclide compositions from the burnup calculation, generate the group constants using a *flat assembly-wide fuel temperature* of 900 K.

There were only three differences in the coupled burnup calculation compared to the uncoupled one:

- Optimization mode 1 was used for Serpent instead of optimization mode 4. This means that the microscopic cross sections were not reconstructed on a unionized energy grid and no pre-calculated macroscopic cross sections were used for the different materials in the simulation.

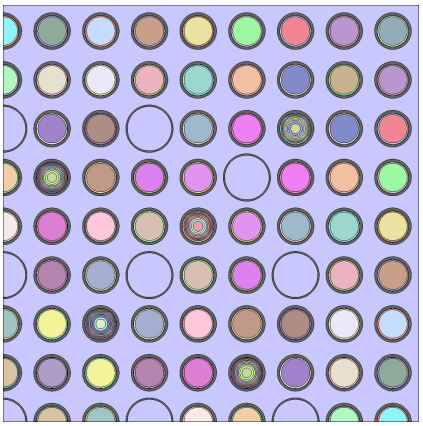

Fig. 4. The depletion zone division shown in the upper right quadrant of the assembly. 1/8 symmetry was utilized in the division.

- The temperature dependence of the cross sections for fuel and cladding was handled on-the-fly with TMS instead of using pre-processed cross section data.

- The temperature distributions for fuel and cladding were provided by the ENIGMA fuel performance code instead of using flat temperature distributions.

No differences are expected to be seen because of the first two variations as the choice of the optimization mode in Serpent does not affect the physics of the solution and is mainly used to modify the trade-off between memory consumption and calculation time and the TMS temperature treatment is known to give reaction rate estimates equivalent with the use of NJOY pre-generated cross sections within statistical accuracy [7].

1. Depletion parameters

The uncoupled and coupled burnup calculations used the same division of the fuel into depletion zones. The 1/8 symmetry of the assembly was utilized in the division so that each unique lattice position was considered as a separate depletion region. The pellet of the burnable absorber (BA) rods was divided into 10 radial rings of equal area, while the pellet of the pure UO_2 rods was divided into two depletion zones to capture the formation of the high burnup structure on the outer rim of the pellet based on studies on the radial subdivision of non-BA rods previously made for the group constant generation in [17]. The outer depletion zone (rim region) in the non-BA rods contained the outermost 0.3 mm of the pellet. The depletion zone division is shown in Fig. 4 in which the outer rim depletion zones of non-BA rods are barely visible.

The depletion history consisted of 53 steps: Two short steps of 0.05 MWd/kgU to the burnup of 0.1 MWd/kgU were followed by a step of 0.40 MWd/kgU to the burnup of 0.50 MWd/kgU. After this, 0.5 MWd/kgU steps were taken until reaching the burnup of 15.0 MWd/kgU, after which the step size was increased to 1.0 MWd/kgU until the burnup of 30.0 MWd/kgU was reached. Further four 2.5 MWd/kgU steps were taken to reach the burnup of 40.0 MWd/kgU followed

by two 5.0 MWd/kgU steps to reach the maximum burnup of 50.0 MWd/kgU.

For the burnup calculation, the SIE-burnup scheme was used with a constant number of 16 iterations for each burnup step. Each inner iteration consisted of 5 active cycles with 125 000 histories per cycle resulting in 10 million active neutron histories per burnup step. The same number of active neutron histories was used also in [17]. For the first transport solution, a flat fission source distribution was used as an initial guess with 40 inactive cycles to allow for source convergence. On subsequent transport solutions, the initial fission source was taken from the last criticality cycle of the previous transport solution. The number of inactive cycles was set to 20 for the first iteration of each burn-up point and to zero for the subsequent inner iterations. Based on a group ($N = 5$) of comparison calculations for one of the history cases, skipping the inactive cycles on the subsequent inner iterations did not produce a statistically significant effect on the final nuclide concentrations.

2. Solution transfer between Serpent and ENIGMA

A small wrapper program handled the solution transfer between Serpent and ENIGMA passing the tallied radial power distribution in each rod to ENIGMA input-files alongside with the information regarding the burnup step length that was needed by ENIGMA to correctly predict the effects of the irradiation on the fuel and cladding thermal and mechanical properties. The wrapper program also read the radial temperature distribution and radial node displacement in the fuel rods from ENIGMA output files and wrote them back to a multi-physics interface that was read by Serpent. The restart capability of ENIGMA was utilized in the coupling, meaning that the ENIGMA solution could be continued from the previously solved burnup point without having to solve the whole irradiation history on each execution. Serpent used the coupled calculation capabilities to signal with the wrapper code at the correct points of the execution of the coupled burnup algorithm (steps 5 and 10 in Table I).

Due to the 1/8 symmetry in the fuel assembly, there were only 39 unique fuel rods. The fuel behavior was solved separately for each of these 39 fuel rods. This included tallying the radial fission power distribution in six rings of equal area for each rod. The radial power distribution was transferred to ENIGMA using a separate power depression file and the fuel temperature and radial node displacement results were read from the ENIGMA *.op8* output-file and transferred to Serpent using the fuel performance code multi-physics interface at 52 radial nodes in the fuel and 3 nodes in the cladding.

V. RESULTS

Typical running times (wall clock time) for the different simulations using typical computing nodes (ProLiant SL390s G7, 2x6 core Intel Xeon X5650 processor) were 6 hours for the uncoupled burnup history (executed on two nodes), 10 hours for the coupled burnup history (executed on four nodes) and 30 minutes for the group constant generation at the 15 burnup points (executed on four nodes)[2].

1. Nuclide concentrations

As was discussed in Section 2., the use of effective temperatures can lead to differences in the local and global nuclide concentrations. This section will examine the differences in the nuclide inventories between the effective temperature burnup calculation and the reference calculation. In order to be able to present the results with some estimates of the associated statistical uncertainties, 10 independent burnup calculations were conducted and the sample mean as well as the sample variance of the mean are shown here.

The relative differences in the concentrations of two important nuclides reflecting the concentrations of fission products and actinides are shown in Figure 5 as a function of burnup. The nuclides shown here are ^{135}I representing the fission products and ^{239}Pu representing the actinides produced by transmutation. The effect of the fuel temperature model on gadolinium depletion is shown in Fig. 6. In addition to presenting the relative differences in assembly total nuclide concentrations (yellow dot) some of the local differences will be presented by looking at the relative differences in the two radial depletion zones of the non burnable absorber rods, namely the outer rim area (red x) and the inner pellet area (green +). The relative differences in total nuclide concentrations in the BA rods are also included (blue circles).

A. Effects on the spatial nuclide distribution

The effective temperature model led to a constant overestimation of the production of ^{239}Pu in the outer area of the fuel pellet combined with a constant underestimation of the production in the inner area of the fuel pellet (Fig. 5 right). The concentrations of other actinides behaved in a similar manner. The plutonium concentration in the BA-rods was overestimated by several percent especially in the early part of the burnup history. All of these changes can be easily associated with differences in the temperatures of the different depletion zones between the effective and the detailed fuel temperature models: The effective fuel temperature is unrealistically high near the surface of the non-BA pellets and unrealistically low in the inner parts of the non-BA fuel pellets. Similarly, the effective temperature is unrealistically high for the BA rods especially before the burnable absorber is depleted. A higher fuel temperature will lead to increased resonance absorption of neutrons by ^{238}U, which directly leads to an increase in the production of ^{239}Pu.

The relative differences between the effective and reference simulations stay quite stable in the center and rim areas of the non BA-rods, which corresponds to a rather constant over- or underestimation of the fuel temperature by the effective temperature model in non BA-rods. In the BA-rods, however, the relative difference between the two models does not stay constant. The shape of the blue curve in Fig. 5 (right) can be compared to the evolution of the volume averaged tem-

[2] A full set of cross sections without control rod branches generated for the core simulator calculations in [5] could typically be generated in under 72 hours.

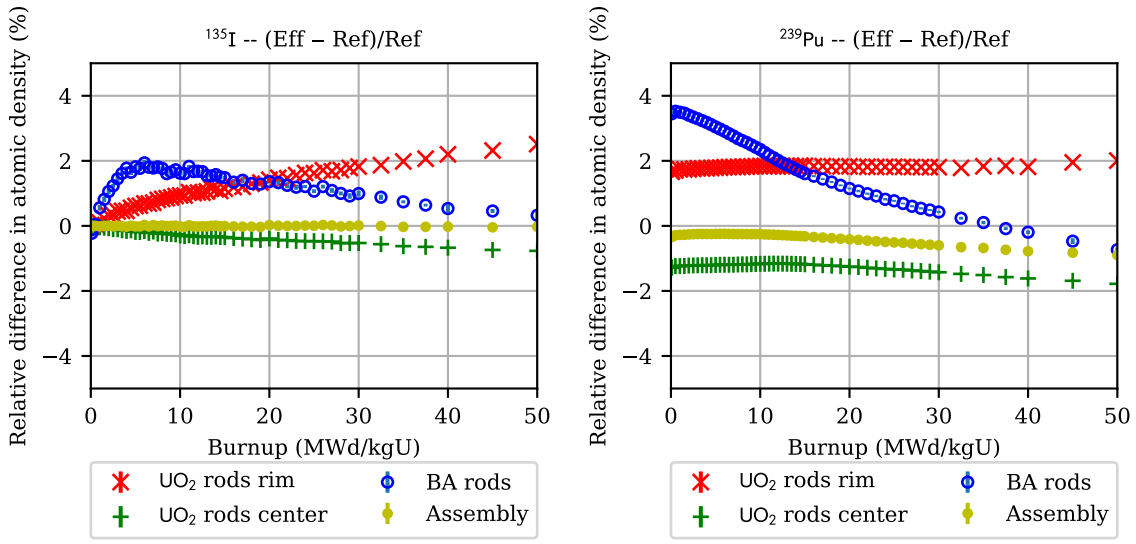

Fig. 5. Relative differences in the concentrations of two nuclides of interest. The trends seen in these two nuclides reflect the general trends seen in other fission products (trends of ^{135}I) and minor actinides (trends of ^{239}Pu). 2σ errorbars. **Left**: ^{135}I a representative non-absorbing fission product with a small total cross section and the precursor of ^{135}Xe, an important parasitic absorber. **Right**: ^{239}Pu an important fissile nuclide transmuted from ^{238}U.

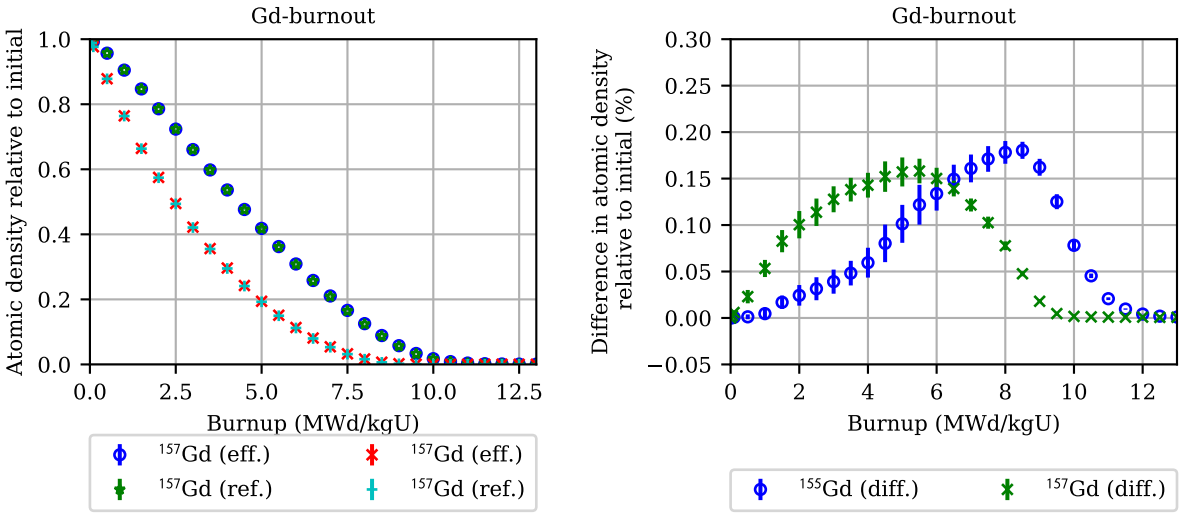

Fig. 6. Isotopic gadolinium burnout with 2σ errorbars. **Left**: The burnout curves for ^{155}Gd and ^{157}Gd in the reference and effective simulations. **Right**: Differences in the isotopic concentrations of the different Gd-isotopes between the two simulations relative to their initial concentrations.

peratures of the Gd-rods shown in Fig. 2. The difference in both the plutonium concentrations and the temperatures starts large, but decreases with increasing burnup. The differences in the average plutonium concentration of the BA-rods reach a minimum slightly before 40 MWd/kgU, close to the same burnup when the volume averaged temperature of the BA-rods reaches 900 K.

The increased concentrations of fissile actinides in the surface areas of the fuel rods as well as in the BA-rods lead to an increase in the fission power at these regions with increasing burnup. This can be seen[3] from the concentrations of the non-absorbing fission product ^{135}I (Fig. 5 left).

B. Effects on gadolinium burnout

The effective temperature model also affects the depletion of the absorbing Gd-isotopes ^{155}Gd and ^{157}Gd from the burnable absorber rods. The left side of Figure 6 shows the burnout of these two nuclides in the two simulations. Of the two isotopes, ^{157}Gd is completely depleted first, near 8.5 MWd/kgU, whereas ^{155}Gd reaches zero concentration after 11 MWd/kgU. While the left side of the figure does not show large differences between the two simulations, plotting the difference in the nuclide concentrations relative to the initial concentrations (Fig. 6 right) shows small but significant differences in the depletion of the two isotopes. The effective temperature calculation results in a slightly slower burnout of both isotopes. The differences in the ^{157}Gd burnout reach their maximum near 5 MWd/kgU while the differences in the ^{155}Gd burnout peak at 8.5 MWd/kgU. The slower burnout of the gadolinium leads to a reactivity difference of almost 100 pcm between the two simulations at 9 MWd/kgU (see Fig. 9, left).

C. Assembly total nuclide inventory

The effective temperature of 900 K reproduces the total amount of fission product nuclides very well. This can be partially attributed to the fact that the amount of fission product nuclides is directly related to the fission rate and the flux level of the system. As both simulations used the same power to deplete the assembly, the fission rates and flux levels also stayed similar to each other[4].

Overall, the effective temperature of 900 K leads to a slightly lower actinide production at the assembly level (see Fig. 5 right for ^{239}Pu, other actinides showed similar trends). To test the dependence of the total actinide production on the value of the effective temperature a second calculation was executed with a higher effective temperature of 950 K. Generally, higher fuel temperature should lead to increased resonance absorption of neutrons by ^{238}U and an increase in the production of actinides. The effect of the higher effective temperature on the fission product and actinide concentrations is shown in Fig. 7: The increase in the effective fuel temperature leads to a slightly stronger overestimation of actinide production and fission power in the rim region, but also results in a larger actinide production overall in a manner that predicts the assembly total ^{239}Pu inventory more accurately throughout the burnup history. This result indicates that a well chosen effective temperature should be able to conserve the total actinide production and prompts questions on a possible method for determining the optimal temperature without having to obtain the accurate reference solution. However, the increased effective temperature does perform worse regarding the gadolinium burnout (Fig. 8).

2. Group constants

Prior to the analysis of the group constants the differences in the development of the assembly reactivity are shown alongside with the flux levels required to reach the power normalization used in the calculations. These parameters are shown in Fig. 9, and while they are not passed to the core simulator they are nevertheless helpful in assessing the effects of the effective temperature calculation. There is a slight underestimation of the assembly reactivity near 10 MWd/kgU burnup, which coincides to the differences seen in the burnout of the gadolinium from the burnable absorber rods. The reactivity difference decreases until 15 Mwd/kgU, after which it increases steadily. The reason for the decreased reactivity at high burnups is the decreased amount of actinides in the assembly when using the effective temperature of 900 K.

To shed further insight into the components of the reactivity difference the homogenized capture and fission neutron production cross sections are presented in Fig. 10. The difference in the reactivity near 10 MWd/kgU seems to be associated with a negative difference in the thermal and fast fission neutron production cross sections at the time combined with a slight overestimation of the thermal capture cross section consistent with the slower burnout of gadolinium. At high burnups, the difference in the fission neutron production cross section increases for both groups as does the difference in the thermal capture cross section. Using an effective temperature of 950 K predicts the behavior of the assembly better at high burnups but has larger discrepancies in the group constants during the gadolinium burnout (not shown here).

For the generated group constants, the largest differences could be seen in the fission cross sections, which were already shown. Fission product yields were predicted well for ^{135}I, ^{135}Xe and ^{149}Pm. However, the yield for ^{149}Sm was underestimated throughout the burnup history (see Fig. 11 left) . ^{135}Xe microscopic absorption cross section (Fig. 11 right) serves as a representative example of the relative differences in the microscopic absorption cross sections of the poison nuclides: The differences are small overall, with a slight overprediction of the fast absorption cross section during the Gd burnout and overprediction in both groups increasing with burnup after Gd-burnout.

Generally the effect of the temperature model on the generated group constants is small. However, the differences in the fission cross section at high burnups may lead to differences in the distribution of power between high burnup and low burnup nodes in full core simulations.

[3] Due to its short half–life of 6.6 h and a small transmutation cross section, ^{135}I serves as a good indicator of the fission power level in the analysis.

[4] This is not always the case even if both simulations use the same power normalization as the average fission energy or the fission or absorption cross sections may diverge due to differences in depletion.

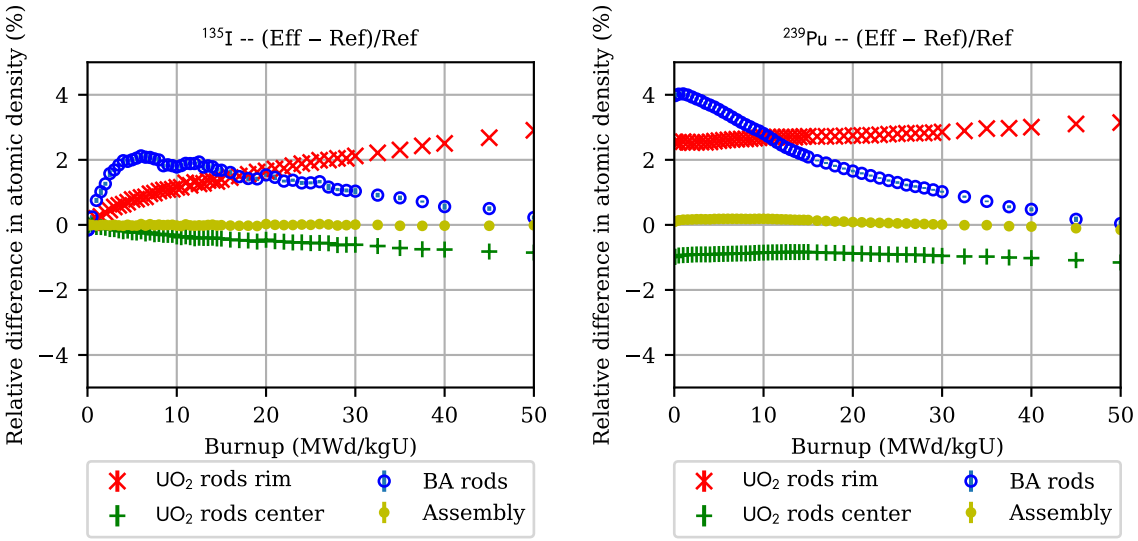

Fig. 7. Relative differences in the concentrations of two nuclides of interest between the **950 K** effective temperature model and reference. 2σ errorbars. **Left**: ^{135}I. Comparison to Fig. 5 (left) shows that increasing the effective temperature to 950 K leads to slightly larger differences in the spatial nuclide distribution (between rim and center). **Right**: ^{239}Pu. Comparison to Fig. 5 (right) shows that increasing the effective temperature to 950 K leads to a more accurate prediction of the assembly-wide ^{239}Pu concentration.

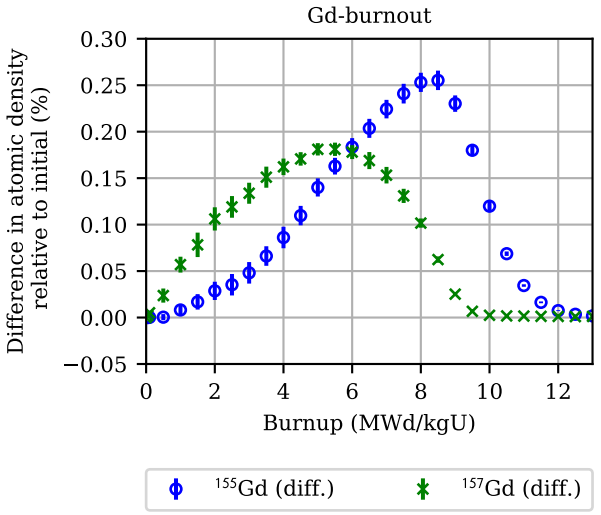

Fig. 8. Differences in gadolinium burnout between the **950 K** effective temperature model and the reference. Comparison to Fig. 6 (right) shows that the effective temperature of 950 K leads to a worse prediction of the Gd burnout compared to the 900 K effective temperature.

VI. RESULTS WITH TWO EFFECTIVE TEMPERATURES

The simulation with an effective temperature of 950 K predicted the actinide production very well but performed worse in the gadolinium burnout than the simulation with a 900 K effective temperature. It is easy to posit that the increased temperature in the BA-rods affects the modeling of the Gd-burnout poorly. Following this line of reasoning, a series of burnup calculations with a separate, lower effective temperature for the BA-rods were conducted. The temperature of the non-BA-rods was kept at 950 K, while the temperature of the BA-rods was varied between 500 and 950 K. The nuclide concentrations obtained from these new effective temperature calculations were again compared to the ones obtained from the reference calculation with realistic temperature distributions provided by the ENIGMA fuel performance code.

It should be noted that, based on the reference simulation, the volume averaged temperature of the BA rods increases roughly from 620 K to 750 K (see Fig. 2) during the gadolinium depletion (between 0 and 11 MWd/kgU).

Decreasing the effective temperature of the burnable absorber rods does bring about an improvement in the modeling of the Gd burnout (Fig. 12). However, even the lowest applied effective temperature of 500 K, which is significantly below the coolant temperature of 583 K, predicts a too slow of a depletion of the two Gd isotopes. This is a surprising result, but may be explained by the fact that the uranium enrichment in the BA-rods is very low (0.25 wt %) which means that even when the gadolinium isotopes are depleted from the fuel, no significant fission power will be produced before some fissile ^{239}Pu has been bred in the BA-rods. As the fission power of the

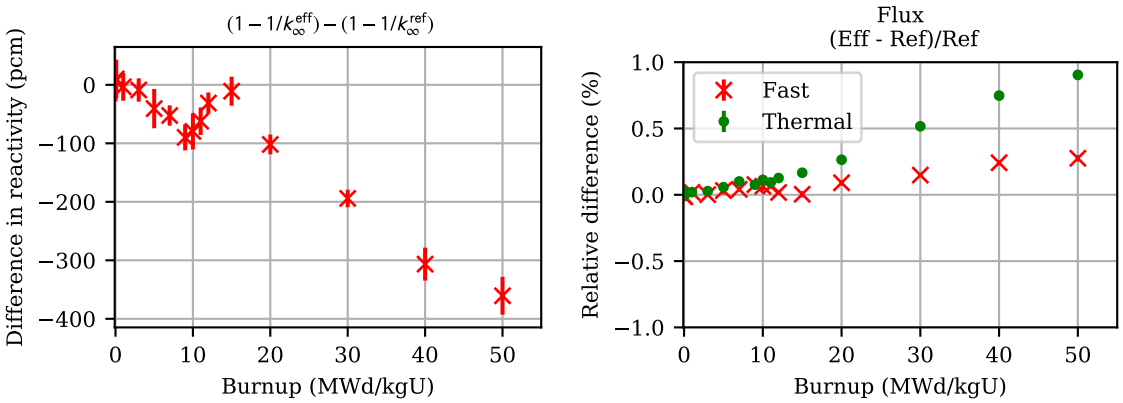

Fig. 9. Relative differences in two parameters obtained from the group constant generation. 2σ errorbars. **Left**: Reactivity of the assembly in the infinite lattice geometry. **Right**: Thermal and fast flux.

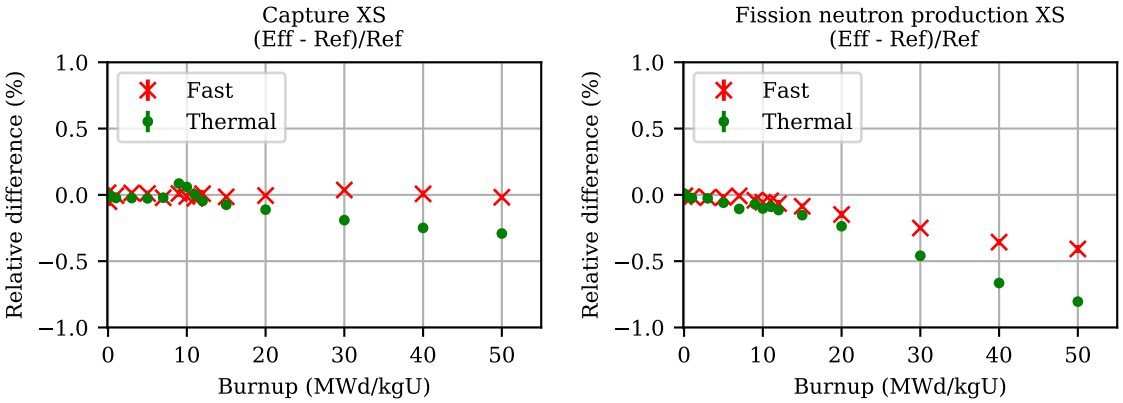

Fig. 10. Relative differences in generated homogenized group constants. 2σ errorbars. **Left**: Capture cross section. **Right**: Fission neutron production cross section.

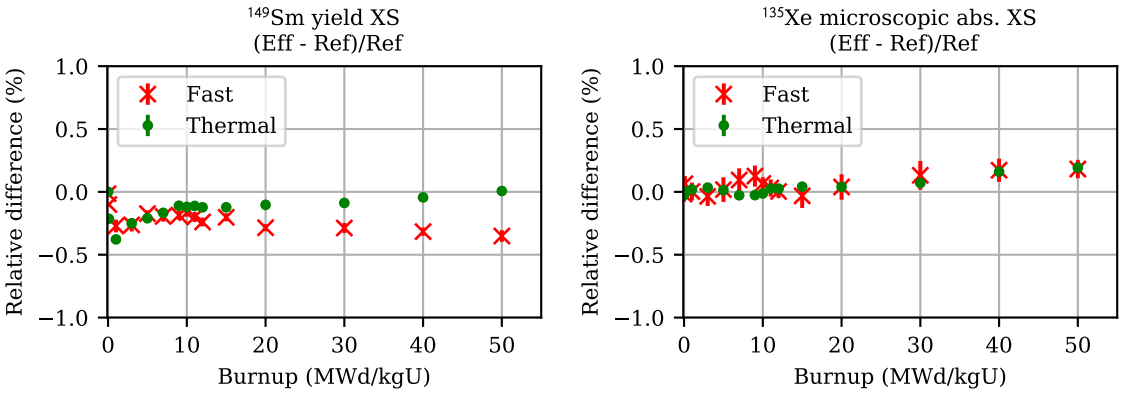

Fig. 11. Relative differences in generated homogenized group constants. 2σ errorbars. **Left**: Microscopic yield for ^{149}Sm. **Right**: ^{135}Xe microscopic absorption cross section.

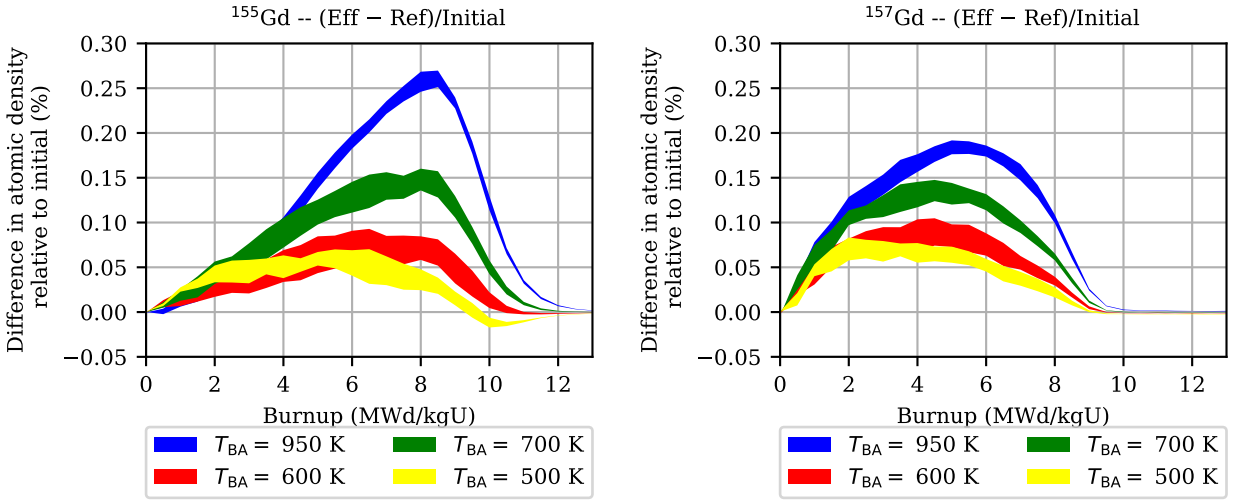

Fig. 12. Differences the gadolinium isotope concentrations relative to their initial concentrations with various effective temperatures for the burnable absorber rods. 2σ shadings. **Left**: ^{155}Gd. **Right**: ^{157}Gd.

BA-rods slowly increases during the Gd-burnout, the breeding of fissile plutonium will also increase due to the increased fuel temperature. As the lower effective temperatures in BA-rods lead to smaller concentrations of fissile ^{239}Pu (See Fig. 13 right), the fission power of the BA-rods will be lower (seen from the concentrations of ^{135}I in Fig. 13 left), which will lead to a reduced neutron flux near the BA-rods and reduced depletion of the burnable absorber.

Decreasing the effective temperature of the BA-rods also decreases the production of actinides at the assembly level (see Fig. 14, right) for ^{239}Pu) and increases the depletion of ^{235}U (Fig. 14, left). This will lead to a reduction in the assembly reactivity at high burnups and will affect the homogenized fission and fission neutron production cross sections, although the detailed analysis of the generated group constants must be left to a separate publication.

VII. CONCLUSIONS

The Stochastic Implicit Euler burnup scheme with thermal feedback was implemented in Serpent 2, which allows the code to consider the effect of realistic fuel temperature distributions on the burnup calculation. This capability was applied in estimating the effects of using effective fuel temperatures in the burnup history part of group constant generation.

The calculations using a single effective temperature for both rods with and without burnable absorber (BA) were able to produce the assembly total concentrations of fission products and actinides very well if a suitable effective temperature was chosen. The spatial distribution of the fission products and actinides between the different radial regions of the fuel rods could not be reproduced with a single radially constant effective temperature. Moreover, a single burnup independent effective temperature could not capture the temperature effects in burnable absorber rods associated with an increase in the fuel temperature after gadolinium burnout and breeding of fissile ^{239}Pu.

The differences in the depletion of the burnable absorber were seen to result in slight differences in the generated group constants between burnups of 5 and 10 MWd/kgU. The differences in assembly wide concentrations of fissile actinides such as ^{239}Pu led to significant differences in the generated group constants at high burnups if an effective temperature of 900 K was used. The effective temperature of 950 K resulted in a better prediction of the generated group constants, but a worse prediction of the gadolinium burnout, which highlights the importance of the effective temperature choice.

None of the effective temperatures used for the burnable absorber rods were able to fully capture the depletion of the two absorbing gadolinium isotopes ^{155}Gd and ^{157}Gd. Similar analysis of assemblies with BA-rods with a higher uranium enrichment should also offer further insight into the problem of determining an effective temperature for burnable absorber rods.

VIII. ACKNOWLEDGMENTS

This work has been funded by the NUMPS project of the Academy of Finland as well as the MONSOON project under the Finnish National Research Programme on Nuclear Power Plant Safety, SAFIR-2014 and SAFIR-2018. The simulations presented above were performed using computer resources within the Aalto University School of Science "Science-IT" project.

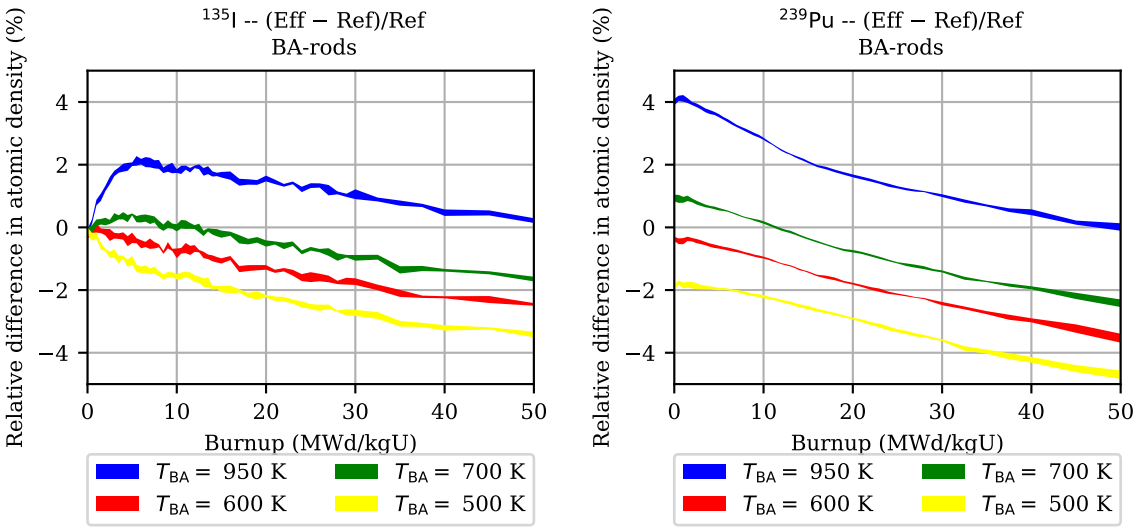

Fig. 13. Differences in the average concentrations of ^{135}I (Left) and ^{239}Pu (Right) in the burnable absorber rods with various effective temperatures for the burnable absorber rods. 2σ shadings.

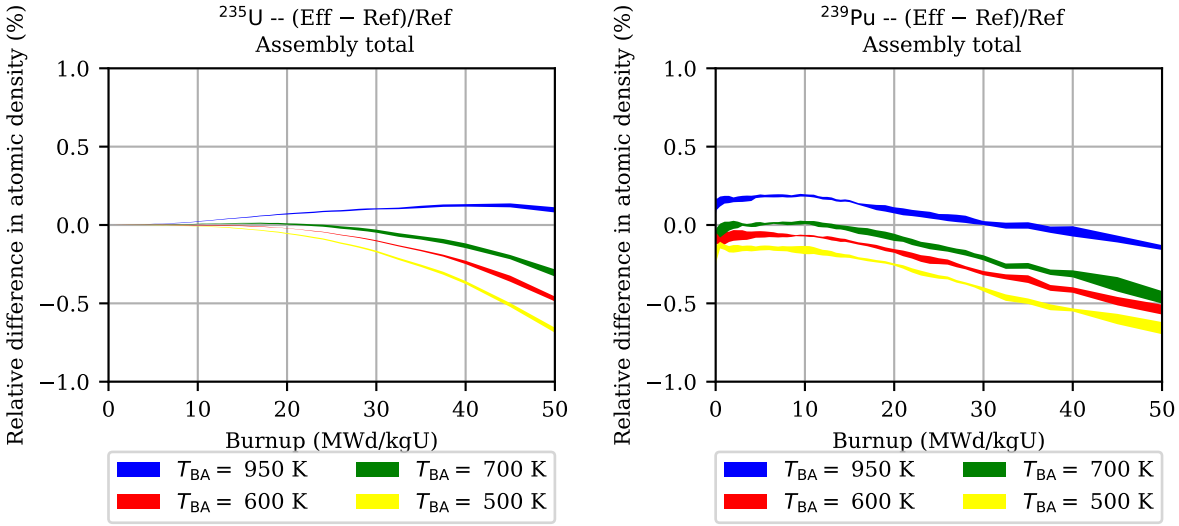

Fig. 14. Differences in the assembly total concentrations of ^{235}U (Left) and ^{239}Pu (Right) with various effective temperatures for the burnable absorber rods. 2σ shadings.

REFERENCES

1. J. LEPPÄNEN, M. PUSA, T. VIITANEN, V. VALTAVIRTA, and T. KALTIAISENAHO, "The Serpent Monte Carlo code: Status, development and applications in 2013," *Annals of Nuclear Energy*, **82**, 142 – 150 (2015).
2. J. DUFEK and H. ANGLART, "Derivation of a stable coupling scheme for Monte Carlo burnup calculations with the thermal-hydraulic feedback," *Ann. Nucl. Energy*, **62**, 260 (2013).
3. G. SENGLER, F. FORÃŁT, G. SCHLOSSER, R. LISDAT, and S. STELLETTA, "EPR core design," *Nuclear Engineering and Design*, **187**, 79 – 119 (1999).
4. R. MATTILA, "Three-dimensional analytic function expansion nodal model," in "Proc. ANFM 2003," Hilton Head Island, SC (5–8 Oct. 2003).
5. V. VALTAVIRTA and J. LEPPÄNEN, "Estimating the Effects of Homogenized Fuel Temperature in Group Constant Generation using Serpent 2," *Annals of Nuclear Energy (submitted)*.
6. J. LEPPÄNEN, M. PUSA, and E. FRIDMAN, "Overview of methodology for spatial homogenization in the Serpent 2 Monte Carlo code," *Annals of Nuclear Energy*, **96**, 126 – 136 (2016).
7. T. VIITANEN, *Development of a stochastic temperature treatment technique for Monte Carlo neutron tracking*, Ph.D. thesis, Aalto University (2015).
8. T. VIITANEN and J. LEPPÄNEN, "New Interpolation Capabilities for Thermal Scattering Data in Serpent 2," in "PHYSOR 2016," Sun Valley, ID, USA (May 1–5 2016).
9. J. LEPPÄNEN, "Modeling of Non-uniform Density Distributions in the Serpent 2 Monte Carlo Code," *Nucl. Sci. Eng.*, **174**, 318 (2013).
10. V. VALTAVIRTA, J. LEPPÄNEN, and T. VIITANEN, "Coupled neutronics–fuel behavior calculations in steady state using the Serpent 2 Monte Carlo code," *Annals of Nuclear Energy*, **100, Part 2**, 50 – 64 (2017).
11. V. VALTAVIRTA, V. TULKKI, J. LEPPÄNEN, and T. VIITANEN, "The Universal Fuel Performance Code Interface in Serpent 2," in "Proc. 2013 Fuel Performance Meeting TopFuel," Charlotte, USA (2013).
12. V. VALTAVIRTA, T. IKONEN, T. VIITANEN, and J. LEPPÄNEN, "Simulating Fast Transients with Fuel Behavior Feedback Using the Serpent 2 Monte Carlo code," in "Proc. Physor 2014," Kyoto, Japan (2014).
13. J. LEPPÄNEN, T. VIITANEN, and V. VALTAVIRTA, "Multi-physics Coupling Scheme in the Serpent 2 Monte Carlo Code." *Trans. Am. Nucl. Soc.*, **107**, 1165 (2012).
14. D. KOTLYAR and E. SHWAGERAUS, "Numerically stable Monte Carlo-burnup-thermal hydraulic coupling schemes," *Annals of Nuclear Energy*, **63**, 371 – 381 (2014).
15. D. KOTLYAR and E. SHWAGERAUS, "Sub-step methodology for coupled Monte Carlo depletion and thermal hydraulic codes," *Annals of Nuclear Energy*, **96**, 61 – 75 (2016).
16. J. DUFEK and V. VALTAVIRTA, "Time step length versus efficiency of Monte Carlo burnup calculations," *Ann. Nucl. Energy*, **72**, 409 (2014).
17. J. LEPPÄNEN and R. MATTILA, "Validation of the Serpent–ARES code sequence using the MIT BEAVRS benchmark – HFP conditions and fuel cycle 1 simulations," *Annals of Nuclear Energy*, **96**, 324 – 331 (2016).